View metadata, citation and similar papers at core.ac.uk
brought to you by CORE
provided by Knowledge Repository of SEMI,CAS

Eur. Phys. J. B **70**, 397–401 (2009)
DOI: 10.1140/epjb/e2009-00237-9

THE EUROPEAN PHYSICAL JOURNAL B

Regular Article

Spin precession and electron spin polarization wave in [001]-grown quantum wells

G.H. Liu[a], Y.H. Chen[b], C.H. Jia, and Z.G. Wang

Key laboratory of semiconductor material science, Institute of semiconductors, Chinese academy of science, P.O. Box 912, Beijing 100083, P.R. China

Received 7 March 2009 / Received in final form 5 May 2009
Published online 15 July 2009 – © EDP Sciences, Società Italiana di Fisica, Springer-Verlag 2009

Abstract. We theoretically study the spatial behaviors of spin precessions modulated by an effective magnetic field in a two-dimensional electron system with spin-orbit interaction. Through analysis of interaction between the spin and the effective magnetic field, we find some laws of spin precession in the system, by which we explain some previous phenomena of spin precession, and predict a controllable electron spin polarization wave in [001]-grown quantum wells. The shape of the wave, like water wave, mostly are ellipse-like or circle-like, and the wavelength is anisotropic in the quantum wells with two unequal coupling strengths of the Rashba and Dresselhaus interactions, and is isotropic in the quantum wells with only one spin orbit interaction.

PACS. 72.25.Dc Spin polarized transport in semiconductors – 71.70.Ej Spin-orbit coupling, Zeeman and Stark splitting, Jahn-Teller effect – 85.75.Hh Spin polarized field effect transistors

In recent years, there has been a great deal of interest in manipulating the spin degrees of freedom in semiconductors due to intriguing physics phenomena that are observed experimentally or predicted theoretically [1–3]. Applying external magnetic fields and magnetic contacts provide a possible approach to control the spin of electron [4]. Of particular interest is the spin manipulation via an adjustment of a gate voltage in semiconductor heterostructures [5–8]. A consequence of the relativity is that the spin and momentum states of an electron can interact in the presence of an electric field, known as spin-orbit interaction. This interaction, just like the interaction between the spin and an effective magnetic field [9,10], opened pathway to the manipulation of electron spins within non-magnetic semiconductors. In general, the effective magnetic field, induced by Rashba spin-orbit interaction (RSOI), is independent of crystallographic direction in which a quantum well has been grown, while the reverse is true for the one induced by Dresselhaus spin-orbit interaction (DSOI). However, the effective magnetic fields are dependent on the strength of spin-orbit interaction and the wave vector. A fascinating feature of RSOI is the fact that its strength can be controlled by a gate voltage. Thus the spin can be purely electrically manipulated in the presence of the spin-orbit interaction. It could be of use in areas from spintronics to quantum computing [5,7,8].

In spintronics, a plenty of theoretical and experimental works [11,18] were stimulated by the Datta-Das spin-field-effect transistor [19], in which the spin precessions are modulated by an effective magnetic field induced by RSOI when electrons are transmitted through a two-dimensional (2D) semiconductor channel. Recently, using an 8×8 Kane model, Winkler has further demonstrated the spatial spin precession in the electron system with spin-orbit interaction [10]. On the other hand, a new spin-field-effect transistor based on spin-orbit coupling of both the Rashba and the Dresselhaus types was proposed [20]. Spin transport through the transistor is tolerant against spin-independent scattering processes. Then a spatial spin precession named persistent spin helix (PSH) was predicted to exist in SU(2)-symmetry quantum wells with equal coupling strengths of the Rashba and Dresselhaus types (RD model) [21]. The PSH is a spetial spin precession pattern with the precession angle depending only on the net displacement along certain directions such as $\pm[110]$. It was also demonstrated by Liu using a contour-integral method [22]. Recently, the PSH has been observed by Koralek et al. using transient spin-grating spectroscopy in [001]-grown quantum wells [23]. A spin polarization wave is generated by the photon helicity wave, and is modulated by an effective magnetic field, and then an ensemble of spins curls into a helix, the collective spin lifetime is greatly enhanced [24], ultimately, a PSH is formed in the two-dimensional electron gas. The experimental demonstration of the persistent spin helix is a remarkable breakthrough, which will be helpful to design spintronic device.

In this paper, through analysis of the competition of two effective magnetic fields induced by RSOI and DSOI

[a] e-mail: liugenhua@semi.ac.cn
[b] e-mail: yhchen@red.semi.ac.cn

respectively, and the interaction between the spin and the total effective magnetic field in a [001]-grown quantum well, we can explain the previous phenomena [21,22,25] of spin precessions and predict some spin precessions which form spin polarization wave (SPW). The SPW, excited by two light beams with crossed-linear polarizations, can form electron spin gratings [26,27] which has been widely used in the study of spin dynamics [26–28], such as spin relaxation and spin diffusion. The SPW, which we find, excited by a linear polarization light beam, can also form electron spin gratings. And the shape of the wave can be controlled by a gate of voltage.

First, we discuss the competition of the two effective fields in a 2D electron system confined in a [001]-grown quantum well made of III–V semiconductor. In crystals lacking an inversion center such as InAs, bulk inversion asymmetry [29] (BIA) results in the DSOI. It inevitably induces an unchangeable effective magnetic field (DEMF). In heterostructures, structure inversion asymmetry (SIA) [30] leads to the RSOI which induces another adjustable effective magnetic field (REMF). The combined effect of the two effective fields determines the properties of the spin precessions in the quantum wells. The system is characterized by the Hamiltonian

$$H_{[001]} = \frac{p_x^2 + P_y^2}{2m^*} + \frac{\alpha}{\hbar}(p_y\sigma_x - p_x\sigma_y) + \frac{\beta}{\hbar}(p_x\sigma_x - p_y\sigma_y), \quad (1)$$

where m^* is the effective electron mass, σ_x and σ_y are the Pauli matrices. The second term of equation (1) originates from the SIA , and the third one originates from the BIA. α and β, assumed to be constant at present, are the Rashba and Dresselhaus strengths, respectively. The eigenfunctions of the system are

$$\Psi_{\uparrow\downarrow} = \frac{1}{\sqrt{2}} e^{(i\vec{k}_{\uparrow\downarrow}\cdot\vec{r})} \begin{pmatrix} ie^{(-i\theta)} \\ \pm 1 \end{pmatrix}, \quad (2)$$

where $\theta = \arg[\alpha\cos\phi + \beta\sin\phi + i(\alpha\sin\phi + \beta\cos\phi)]$, $k_\uparrow$ and $k_\downarrow$ are the vectors of spin-up and -down electron, respectively. The corresponding eigenenergies are

$$E_{\uparrow\downarrow} = \frac{\hbar^2 k^2}{2m^*} \pm \xi(\alpha,\beta,\phi)k, \quad (3)$$

where

$$\xi(\alpha,\beta,\phi) = \sqrt{\alpha^2 + \beta^2 + 2\alpha\beta\sin(2\phi)}, \quad (4)$$

here ϕ is the argument angle of $\vec{k} \equiv (k_x, k_y) = k(\cos\phi, \sin\phi)$. We assume that $E_\uparrow = E_\downarrow = E$, and then we obtain

$$k_{\uparrow\downarrow} = \frac{\pm m^*\xi + m^*\sqrt{\xi^2 + 2\hbar^2 E/m^*}}{\hbar^2}. \quad (5)$$

In accordance with references [9] and [10], the effective magnetic field can be defined as $\vec{B} = \Delta k\langle\Psi_\uparrow|\vec{\sigma}|\Psi_\uparrow\rangle$ when the wave vector is sufficiently small ($k < 10^8$ m^{-1}), where $\Delta k = \frac{2m^*\xi}{\hbar^2}$. So these effective magnetic fields in the system can be expressed as

$$\vec{B}_{SIA} = \frac{2m^*\alpha}{\hbar^2}(\sin\phi, -\cos\phi, 0) \quad (6)$$

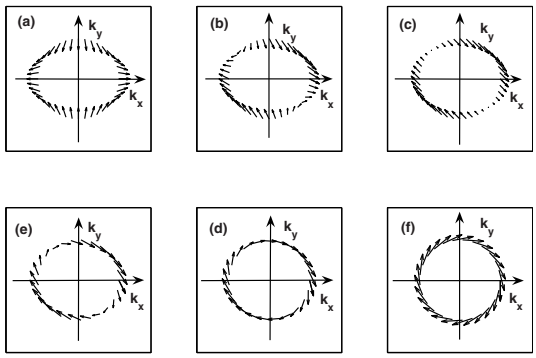

Fig. 1. Effective magnetic fields with (a) ratio = 0, (b) ratio = 0.5, (c) ratio = 1, (d) ratio = 2, (e) ratio = 4, and (f) ratio = ∞, i.e., $\beta = 0$.

for REMF,

$$\vec{B}_{BIA} = \frac{2m^*\beta}{\hbar^2}(\cos\phi, -\sin\phi, 0) \quad (7)$$

for DEMF,

$$\vec{B}_{total} = \vec{B}_{SIA} + \vec{B}_{BIA} = \frac{2m^*\xi(\alpha,\beta,\phi)}{\hbar^2}(\sin\theta, -\cos\theta, 0) \quad (8)$$

for the total effective magnetic field in the system. Note that when we fix coupling strengths α, β, these effective magnetic fields are determined by the direction of wave vector (ϕ), and independent of its magnitude. We also note that the fields have a rotational symmetry, i.e., $\vec{B}_{total}(\phi) = -\vec{B}_{total}(\phi+\pi)$. The total fields $\vec{B}_{total}$ with different ratio of α to β are plotted in Figure 1 which exhibits their rotational symmetry in the momentum space. With the increase of the ratio, the symmetry of fields gradually transits from $\vec{B}_{BIA}$ to $\vec{B}_{SIA}$, but all the magnitudes of the fields exhibit axial symmetry around the [$\bar{1}$10] axis. We show the directions of the effective fields only for a circle in the k_x-k_y plane, because these results are typical, for circles with different radii only trivial changes occur.

In Figure 2, the calculated magnitude of the field $\vec{B}_{total}$ is plotted as a function of the ratio α/β and the argument angle ϕ in polar coordinates, where the radius stands for the ratio. The figure distinctly shows axial symmetries of the field, and we label its two symmetry axes with two dash arrows. The magnitude of $\vec{B}_{total}$ behaves as a periodic function of the argument angle ϕ, the period is π. In addition, for a fixed ratio α/β, the field reaches a maximum when $\phi = \pi/4$ or $5\pi/4$, and a minimum when $\phi = 3\pi/4$ or $7\pi/4$. The reason is that the direction of $\vec{B}_{BIA}$ is same as that of $\vec{B}_{SIA}$ at $\phi = \pi/4$ or $5\pi/4$, but opposite to that of $\vec{B}_{SIA}$ at $\phi = 3\pi/4$ or $7\pi/4$ (see Figs. 1a and 1f). With the increase of the ratio, the magnitude of the field first decreases and then increases at $\phi = 3\pi/4$ or $7\pi/4$, and the minimum is zero when the ratio is 1, because $\vec{B}_{BIA} = -\vec{B}_{SIA}$ at the two argument angles.

In what follows, we consider the spin precessions in the above systems, a spin with polar angle θ_s (the angle

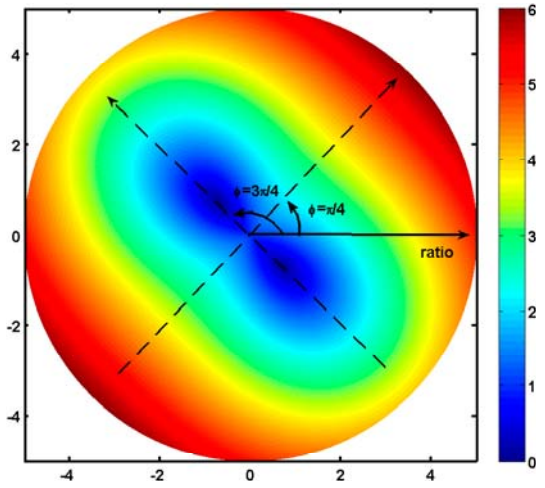

Fig. 2. (Color online) The calculated magnitude of $\vec{B}_{total}$ is plotted as a function of the ratio and the argument angle ϕ in polar coordinates. The radius stands for the ratio, and the unit of the $\vec{B}_{total}$ is $2m^*\beta/\hbar^2$.

between the spin and z direction) and azimuthal angle φ_s (the angle between the spin and x direction) is injected at the origin of (0, 0) coordinates. Using the equations $[\sigma_x, H] = 2i(\alpha k_x + \beta k_y)\sigma_z$, $[\sigma_y, H] = 2i(\alpha k_y + \beta k_x)\sigma_z$, and $[\sigma_z, H] = -2i(\alpha k_x + \beta k_y)\sigma_x - 2i(\alpha k_y + \beta k_x)\sigma_y$, the Heisengberg equation of motion $i\hbar\dot{\sigma}_i = [\sigma_i, H]$ can be solved to obtain the spin expectation values [22]

$$\langle\sigma_x\rangle_t = [\langle\sigma_z\rangle_0 \sin\omega t - (\langle\sigma_x\rangle_0 \cos\theta + \langle\sigma_y\rangle_0 \sin\theta) \times (1 - \cos\omega t)]\cos\theta + \langle\sigma_x\rangle_0, \quad (9)$$

$$\langle\sigma_y\rangle_t = [\langle\sigma_z\rangle_0 \sin\omega t - (\langle\sigma_x\rangle_0 \cos\theta + \langle\sigma_y\rangle_0 \sin\theta) \times (1 - \cos\omega t)]\sin\theta + \langle\sigma_y\rangle_0, \quad (10)$$

$$\langle\sigma_z\rangle_t = \langle\sigma_z\rangle_0 \cos\omega t - (\langle\sigma_x\rangle_0 \cos\theta + \langle\sigma_y\rangle_0 \sin\theta)\sin\omega t, \quad (11)$$

with $\langle\sigma_x\rangle_0 = \sin\theta_s\cos\varphi_s$, $\langle\sigma_y\rangle_0 = \sin\theta_s\sin\varphi_s$, $\langle\sigma_z\rangle_0 = \cos\theta_s$, and $\omega t = 2kt\xi/\hbar$. We note that the group velocity is

$$v = \frac{1}{\hbar}\frac{\partial E}{\partial k}. \quad (12)$$

Using equations (3) and (12), we obtain

$$\frac{\hbar k}{m} = v \mp \frac{\xi}{\hbar^2}, \quad (13)$$

we set

$$v\pm = v \mp \frac{\xi}{\hbar^2}. \quad (14)$$

Substituting equations (13) and (14) into $\omega t = 2kt\xi/\hbar$, one can obtain

$$\begin{aligned}\omega t &= 2m^* v_\pm t\xi/\hbar^2 \\ &= 2m^* r\xi/\hbar^2 \\ &= \triangle kr.\end{aligned} \quad (15)$$

In presence of spin orbit coupling, $v_+ \neq v_-$, which means that the spin-up electron will lag behind the spin-down electron when they travel a same distance. But they obtain same phase difference $\triangle kr$. The above deduction is an approximate process because we assume the electron is a free particle. A strict deduction was given by Liu using a contour-integral method [25]. The above equations demonstrate that the phase of spin depends on its displacement of electron and the difference of wave vectors. Both spin-up and -down state follow the spatial evolution law [22].

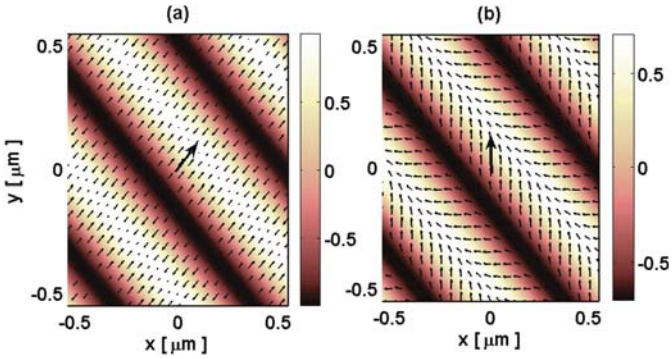

Fig. 3. (Color online) PSH patterns in a 2D electron system for RD model with (a) $\varphi_s = \pi/4$, (b) $\varphi_s = \pi/2$. Arrows express the component of $\langle\vec{\sigma}\rangle$ in the x-y plane. Color bar calibrates $\langle\vec{\sigma}_z\rangle$ with the unit $\hbar/2$. All the injection points are (0, 0), and the injected spins are shown by the bold arrows in (a) and (b).

The overlap of the spin vector with the field $\vec{B}_{total}$ is given by

$$\vec{B}_{total}\cdot\langle\vec{\sigma}\rangle = \frac{2m^*\xi(\alpha,\beta,\phi)}{\hbar^2}\sin(\theta-\varphi_s)\sin\theta_s. \quad (16)$$

So when $\vec{B}_{total}\cdot\langle\vec{\sigma}\rangle = 0$, i.e., $\theta_s = n\pi$, or $\theta - \varphi_s = n\pi$ (n is an integer), equation (16) is independent of the spatial position of the 2D electron system. The spin of injection will be always perpendicular to and precess around the field $\vec{B}_{total}$. On the other hand, when $\vec{B}_{total}\cdot\langle\vec{\sigma}\rangle \neq 0$, i.e., $\theta_s \neq n\pi$ and $\theta - \varphi_s \neq n\pi$, the spin of injection will precess on a cone around the field $\vec{B}_{total}$, where the cone angle is $|\pi/2 - \theta + \varphi_s|$ or $\pi - |\pi/2 - \theta + \varphi_s|$.

Using the above law, we can easily explain the PSHs found by Bernevig et al. [21,22]. Figure 3a shows the special case in an InAs-based 2D electron system. The parameters are taken as $\alpha = \beta = 1.062 \times 10^{-2}$ eV nm, and $m^* = 0.023\ m_0$, where m_0 is the electron rest mass, and the spin orientation of the injection point (0, 0) is set as $\theta_s = \pi/2$ and $\varphi_s = \pi/4$. Due to the equal coupling strengths of the Rashba and Dresselhaus interactions in RD model, $\theta = \pi/4$. So we can easily deduce that $\vec{B}\cdot\langle\vec{\sigma}\rangle = 0$, indicating that the spin will be always perpendicular to and precess around the field $\vec{B}_{total}$ when the electron propagates in the quantum well. Because the directions of the field are constant, pointing to either $[\bar{1}10]$ or $[1\bar{1}0]$, we can see that the spins rotate along the directions $\pm[110]$ in Figure 3a. Furthermore, the antisymmetry of PSH reflects the antisymmetry of the field which has been plotted in Figure 1c. A more general PSH in the system

$$(\kappa\lambda)^2 = \frac{2(\frac{\hbar^2\kappa\pi}{m^*(\alpha+\beta)})^2(\frac{\hbar^2\kappa\pi}{m^*(\alpha-\beta)})^2}{(\frac{\hbar^2\kappa\pi}{m^*(\alpha+\beta)})^2 + (\frac{\hbar^2\kappa\pi}{m^*(\alpha-\beta)})^2 - ((\frac{\hbar^2\kappa\pi}{m^*(\alpha-\beta)})^2 - (\frac{\hbar^2\kappa\pi}{m^*(\alpha+\beta)})^2)cos(2(\phi+\pi/4))}. \quad (17)$$

is plotted in Figure 3b. We set the spins as $\theta_s = \pi/2$ and $\varphi_s = \pi/2$ at the injection point, other parameters are the same as above. It is shown that the spins precess around the effective magnetic field $\vec{B}_{total}$ with a cone angle $\pi/4$ or $3\pi/4$. Due to the properties of the field, these PSHs exhibit a special spin precession pattern with the precession angle depending only on the net displacement in certain directions $\pm[110]$, as shown in Figures 3a and 3b.

In addition, the spatial spin precessions discussed by Liu [25] also reflect the law in [001]-grown quantum wells. From equation (8), the direction of $\vec{B}_{total}$ can be expressed as $(\sin\theta, -\cos\theta, 0)$. When the ratio $\alpha/\beta = 2.15$, we can obtain $\theta_{\phi=\pi/4} = \pi/4$, and the cone angle $|\pi/2 - \theta + \varphi_s|_{\varphi_s=\pi/4} = \pi/2$. It indicates that the injected spin will be always perpendicular to and precess around $\vec{B}_{total}$ when it propagates along the [110] direction in the quantum well. We can also obtain $\theta_{\phi=0} \approx 5\pi/36$, and the cone angle $|\pi/2-\theta+\varphi_s|_{\varphi_s=\pi/4} = 11\pi/18$, which indicates that when a spin propagates along the [100] direction, it will precess on a cone around the effective magnetic field $\vec{B}_{total}$, where the cone angle is $11\pi/18$. These spin precessions were shown in reference [25].

Now, we consider the spatial behaviors of spin precessions in a [001]-grown quantum well with different ratios between α and β. In order to meet the condition $\vec{B}_{total} \cdot \langle\vec{\sigma}\rangle = 0$, a z direction spin is assumed to be injected at the origin of (0, 0) coordinates. Some interesting spin precession patterns generate in this system plotted in Figure 4. The spin precessions form spin polarization waves which propagate in the quantum well, like water wave. The spatial behaviors of $\langle\sigma_z\rangle$ exhibit elliptical or circular symmetry when $\alpha \neq \beta$, and all the ellipses have same symmetry axes [110] and $[\bar{1}10]$, which indirectly reflects the symmetry of the field $\vec{B}_{total}$ in the system (see Figs. 1 and 2). In addition, the spins, injected at the origin of (0, 0) coordinates , will return exactly to the original orientation when they propagate to the brightest ellipses or circles, and turn to the reverse direction when they propagate to the darkest ellipses or circles as shown in the figures. The wavelength of the SPW is anisotropic in the quantum wells when $\alpha \neq \beta$ (see Figs. 4b and 4c). We also note that the wavelength is isotropic in the quantum wells with only one spin orbit interaction (see Figs. 4a and 4d). Physically, these behaviors can be understood from the period of the spin expectation value $\langle\sigma\rangle$. The three equations (9), (10) and (11) can be expressed as the form $\langle\sigma_i\rangle = A\cos(2m^*r\xi/\hbar^2 + \vartheta) + C$, where $i = x, y, z$. So the wavelength of the SPW for $\langle\sigma_z\rangle$ is $\lambda = \frac{\hbar^2\pi}{m^*\xi}$. Substituting equation (4) into the wavelength, we can obtain

see equation (17) above

where $\kappa = n$ or $\kappa = n + 1/2$, n is a positive integer. The equation indicates that the distribution of the $\kappa\lambda$ is an ellipse or circle in the real plane when $\alpha \neq \beta$. The major semi-axis of the ellipse is $\frac{\hbar^2\kappa\pi}{m^*(\alpha-\beta)}$, and the minor semi-axis of the ellipse is $\frac{\hbar^2\kappa\pi}{m^*(\alpha+\beta)}$. The $\cos(2(\phi+\pi/4))$, being a part of the equation, indicates that the symmetry axes of the ellipse are axes [110] and $[\bar{1}10]$. Particularly, when $\alpha = 0$ or $\beta = 0$, the distribution of λ is a circle. When $\kappa = n$, equation (17) describes these brightest ellipses or circles in Figure 4. In addition, when $\kappa = n + 1/2$, equation (17) describes these darkest ellipses or circles in Figure 4. This is why we can see that the spin of injection can return exactly to the original orientation after propagating to these brightest ellipses or circles, and turn to reverse direction after propagating to these darkest ellipses or circles. we also note that the positions of the major semi-axis and the minor semi-axis exchange when the ratio between α and β is less than zero (i.e., $\alpha < 0$).

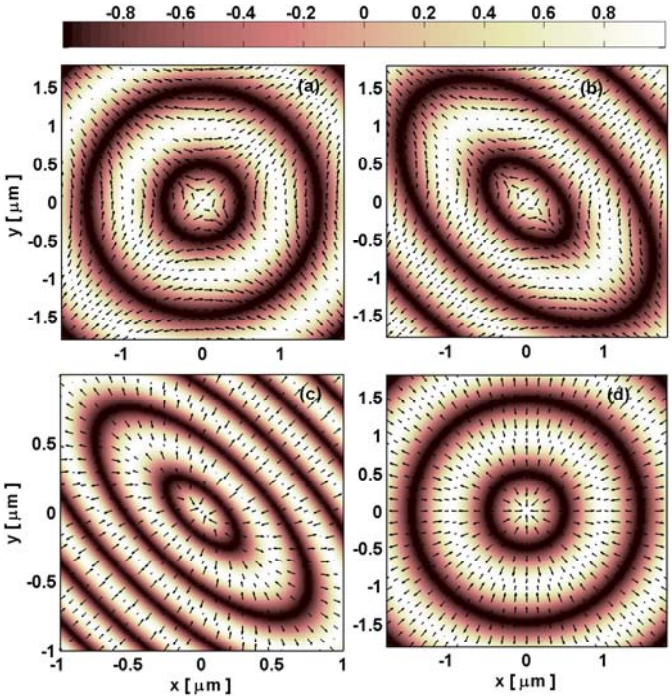

Fig. 4. (Color online) Spin precessions with a fixed DSOI stength $\beta = 1.062 \times 10^{-2}$ eV nm and different ratios (α/β) for (a) 0; (b) 0.25; and (c) 2.5; (d) ratio $= \infty$ ($\alpha = 1.062 \times 10^{-2}$ eV nm and $\beta = 0$). Arrows express the component of $\langle\vec{\sigma}\rangle$ in the x-y plane. Color bar calibrates $\langle\vec{\sigma}_z\rangle$ with the unit $\hbar/2$, all the injection points are (0, 0).

Using equation (17), we can obtain these elliptical eccentricity $e = 2\sqrt{\frac{\alpha}{\beta}}/(1+\frac{\alpha}{\beta})$. Figure 5 shows the eccentricity as a function of the ratio α/β for the [001]-grown quantum wells. With increase of the ratio, the eccentricity first increases, then decreases. when $\alpha = \beta$, the eccentricity

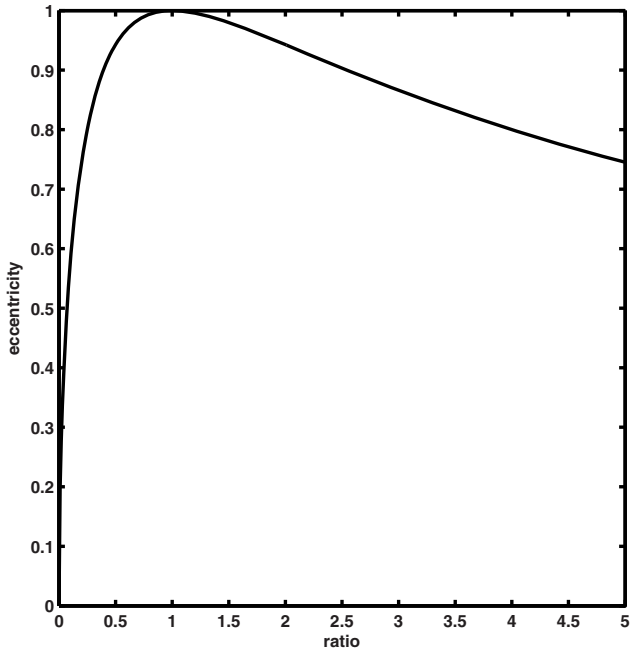

Fig. 5. The eccentricity of the ellipse vs the ratio between α and β.

reaches the maximum 1, it indicates that equation (17) are no more an elliptical equation. The reason is that there are no effective magnetic fields to manipulate the spin in the directions $[\bar{1}10]$ and $[1\bar{1}0]$ due to $\vec{B}_{total}|_{\phi=3\pi/4,7\pi/4} = 0$ in the RD model.

Moreover, the SPW, excited by two spatial modulation light beams with crossed-linear polarizations, forms electron spin gratings which has been widely used in the measure of spin transport and relaxation [26–28]. The SPWs found in this paper, are easy to generate and control. We only need a linear polarization light pulse to excite electron with z direction spin, or we directly inject the electrons applying ferromagnet. The shapes of the wave can be modulated by RSOI which is controlled by a gate voltage. Therefore the SPW can form electron spin gratings in various shapes. The SPWs can be demonstrated using Kerr rotation microscopy.

In summary, we have studied the spin precession in a 2D electron system with spin-orbit interaction. Through analysis of the competition of two effective magnetic fields and the interaction between the spin and the effective magnetic field, we find some laws for the spatial spin precessions in [001]-grown quantum wells. When the injected spins are transmitted through the 2D electron gas, they will precess on a cone around the effective magnetic field $\vec{B}_{total}$, where the cone angle is $|\pi/2 - \theta + \varphi_s|$ or $\pi - |\pi/2 - \theta + \varphi_s|$. In addition, we predict a controllable spin polarization wave in the 2D system. The shape of the wave is controlled by the strength of RSOI and DSOI. Our results may be helpful to the detection and manipulation of electron spins within non-magnetic semiconductors.

The work was supported by the 973 program (2006CB604908, 2006CB921607), and the National Natural Science Foundation of China (60625402).

References

1. D. Awschalom, M. Flatté, Nature Phys. **3**, 153 (2007)
2. I. Žutić, J. Fabian, S. Das Sarma, Rev. Mod. Phys. **76**, 323 (2004)
3. J. Li, B.Q. Huang, I. Appelbaum, Appl. Phys. Lett. **92**, 142507 (2008)
4. G.A. Prinz, Science **282**, 1660 (1998)
5. Y. Kato, R.C. Myers, A.C. Gossard, D.D. Awschalom, Nature (London) **427**, 50 (2004)
6. J. Könemann, R.J. Haug, D.K. Maude, V.I. Fal'ko, B.L. Altshuler, Phys. Rev. Lett. **94**, 226404 (2005)
7. J. Fabian, A. Matos-Abiague, C. Ertler, P. Stano, I. žutić, Acta Phys. Slovaca **57**, 565 (2007), `arXiv:0711.1461`
8. *Semiconductor Spintronics and Quantum Computation*, edited by D. Awschalom, D. Loss, N. Samarth (Springer, New York, 2002)
9. R. Winkler, *Spin-Orbit Coupling Effects in Two-Dimensional Electron and Hole Systems* (Springer, Berlin, 2003)
10. R. Winkler, Phys. Rev. B **69**, 045317 (2004)
11. X.F. Wang, P. Vasilopoulos, F.M. Peeters, Appl. Phys. Lett. **80**, 1400 (2002)
12. P. Gallo, A. Arnoult, T. Camps, E. Havard, C. Fontaine, J. Appl. Phys. **101**, 024322 (2007)
13. J. Wan, M. Cahay, S. Bandyopadhyay, J. Appl. Phys. **102**, 034301 (2007)
14. S. Caliskan, J. Phys.: Condens. Matter **18**, 10313 (2006)
15. S. Caliskan, M. Kumru, J. Phys.: Condens. Matter **19**, 076205 (2007)
16. S.Q. Shen, Z.J. Li, Z.S. Ma, Appl. Phys. Lett. **84**, 996 (2004)
17. K.M. Jiang, Z.M. Zheng, Baigeng Wang, D.Y. Xing, Appl. Phys. Lett. **89**, 012105 (2006)
18. I. Appelbaum, D.J. Monsma, Appl. Phys. Lett. **90**, 262501 (2007)
19. S. Datta, B. Das, Appl. Phys. Lett. **56**, 665 (1990)
20. J. Schliemann, J.C. Egues, D. Loss, Phys. Rev. Lett. **90**, 146801 (2003)
21. B.A. Bernevig, J. Orenstein, S.C. Zhang, Phys. Rev. Lett. **97**, 236601 (2006)
22. M.H. Liu, K.W. Chen, S.H. Chen, C.R. Chang, Phys. Rev. B **74**, 235322 (2006)
23. J.D. Koralek, C.P. Weber, J. Orenstein, B.A. Bernevig, S.-C. Zhang, S. Mack, D.D. Awschalom, Nature (London) **458**, 610 (2009)
24. J. Fabian, Nature (London) **458**, 580 (2009)
25. M.H. Liu, C.R. Chang, S.H. Chen, Phys. Rev. B **71**, 153305 (2005)
26. A.R. Cameron, P. Riblet, A. Miller, Phys. Rev. Lett. **76**, 4793 (1996)
27. C.P. Weber et al., Nature (London) **437**, 1330 (2005)
28. S.G. Carter et al., Phys. Rev. Lett. **97**, 136602 (2006)
29. G.F. Dresselhaus, Phys. Rev. **100**, 580 (1955)
30. Yu.A. Bychkov, E.I. Rashba, J. Phys. C **17**, 6039 (1984)